AC analysis of defect cross sections using non-radiative MPA quantum model

Davide Garetto*[†], Yoann Mamy Randriamihaja[‡], Alban Zaka[‡],
Denis Rideau[‡], Alexandre Schmid[†], Hervé Jaouen[‡], and Yusuf Leblebici[†]

*IBM Systems and Technology Group - 850, rue Jean Monnet, Crolles, France - Email: david.garetto@fr.ibm.com
[†]Ecole Polytechnique Fédérale de Lausanne - Lausanne, Switzerland
[‡]STMicroelectronics - Crolles, France

Abstract— **A multiphonon-assisted model included in a Poisson-Schroedinger solver has been applied for the calculation of the capture/emission trapping rates of Si/SiO$_2$ interface defects and their dependence with respect to the trap energy and depth in the oxide. The accurate trap cross-sections extracted with this approach permit compact modeling engineers to evaluate the accuracy of constant cross-section models. The model has been applied to extract the trap concentration and frequency response, comparing AC simulations with measurements.**

Index Terms—**trap cross-section, multiphonon trapping model, AC analysis**

I. INTRODUCTION

The degradation of the oxide layers and Si/SiO$_2$ interfaces in MOS devices is responsible of uncontrolled parameter variations, performance modification and general device lifetime reduction [1] [2]. For these reasons, physical models describing the oxide degradation mechanisms and the effects of defects are growing in importance in modern nanoscale technologies [3] [4] [5].

The most common example of interfacial point defects is represented by a sp^3-like silicon dangling bond at the interface [6] and has been historically characterized using Electron Paramagnetic Resonance (EPR) spectroscopy [7], [8]. The amphoteric nature of P_b centers is responsible of the altered electrical characteristics. Indeed, Si dangling bonds act both as electron donors and acceptors, having two allowed energy levels in the Si/SiO$_2$ bandgap of the interface, corresponding to a positive and negative charge state. The importance of knowing the P_b-center density relies in its close relationship with the total interface state density affecting the channel charge [8], [9].

The relation between microscopic physical analysis and macroscopic effects on the electrical characteristics is still under debate [10]. The recent correlation found between Random telegraph noise (RTN) and Negative Bias Temperature Instability (NBTI) recovery by considering interface and oxide defects having a wide spread distribution of capture/emission times [11], showed that the trapping dynamics of single defects is playing a major role in the phenomena [10]. For this reason, increasing effort has been performed to determine the relationship between the macroscopic time constants and the microscopic variables predicted by multiphonon theory and associated to the tunneling interaction between the carrier reservoirs, e.g. the channel, and the point defect position.

Compact approaches rely on effective trap cross-sections to model the capture/emission tunneling probabilities, but the dependence on temperature, electrical field and trap energy are often neglected or modeled with empirical parameters [12]. The capture and emission times representing the probabilities of capturing/emitting a carrier from/to the carrier position have been attributed to multiphonon-assisted transitions [13] and quantum models have been proposed to determine the transition probabilities between the channel states and a neutral trap level [3].

In this work a multiphonon-assisted trapping model has been integrated into a Poisson-Shroedinger (PS) solver and used to investigate the dynamics of charge trapping and the capture/emission times for both electrons and holes in different operating regimes. In the following, the details of the model description, the calculation of capture/emission frequencies as well as the effective trap cross-sections and its correlation with AC measurements results will be given.

II. MODEL DESCRIPTION

A 1D multiphonon-assisted trapping model included in a self-consistent Poisson-Schroedinger k.p solver [14] has been adopted. The small signal model proposed in [15] has been applied to perform DC and AC analysis, while the theory of non-radiative capture/emission of carriers by multi–phonon processes is assumed for the calculation of the trap capture/emission events. To include the trapped charge ρ_T in the Poisson iteration, the model determines the quasi-Fermi level E_F at the trap position x in the structure by solving the rate equation,

$$N_T(x, E_T)\frac{\partial f_T(x, E_T, E_F, t)}{\partial t} = \Phi_c(x, E_T, t) - \Phi_e(x, E_T, t) + \tilde{\Phi}_e(x, E_T, t) - \tilde{\Phi}_c(x, E_T, t) \quad (1)$$

where $N_T(x, E_T)$ is the trap distribution in the oxide layer, E_F is the quasi Fermi level to be calculated, Φ_c/Φ_e ($\tilde{\Phi}_c/\tilde{\Phi}_e$) are the capture/emission fluxes from the reservoir to the trap position for e^- (h^+, respectively) and f_T represents the trap occupation. The equation has been solved in steady-state conditions ($\partial f_T/\partial t = 0$) and in the Fourier domain for AC analysis.

The dynamics of multiphonon trapping and tunneling mechanisms are included in the e^- capture/emission frequencies τ_C^{-1}/τ_E^{-1} as discussed in [14]. These characteristic frequencies used in the calculation of the fluxes Φ can be determined with

$$\tau_C^{-1}(x, E_T, t) = \int_{\mathbf{k}} W_C(x, \mathbf{k}, E_T, t)f(x, \mathbf{k}, t)d\mathbf{k}$$
$$\tau_E^{-1}(x, E_T, t) = \tau_C^{-1}(x, E_T, t)e^{\frac{E_T - \mathcal{E}}{k_B T}} \quad (2)$$

by knowing the channel carrier distribution f and the capture probabilities

$$W_c(x, \mathcal{E}, E_T) = \frac{2\pi}{\hbar} R(\Delta E)|V|^2 \exp\left(\frac{F^2}{F_C^2}\right)$$
$$\left[rS\left(1 - \frac{\Delta E}{\hbar\omega S}\right)^2 + (1-r)\sqrt{\left(\frac{\Delta E}{\hbar\omega S}\right)^2 + 4\overline{n}(\overline{n}+1)}\right] \quad (3)$$

A critical electric field F_C has been introduced to take into account the bias dependence of the capture/emission rates at high voltages. Huard [16] and Grasser [10] showed that a constant field $3MV/cm$ well agrees with the capture rates measured using TDDS over

different CMOS technologies. The Huang-Rhys factor S and the phonon frequency ω have been taken constant to values measured by [17] on the entire oxide layer (S=9.6 and $\hbar\omega = 39.2 meV$). A billiard-ball model [12] has been used for calculating the trap wavefuction, while the energetic levels and the carrier wavefunctions determined by the Schroedinger solution within the effective mass approximation are used. Other terms of Eq 3 are defined in [14]. The amphoteric nature of P_b centers (neutral when unoccupied and having the possibility to capture a h^+ or an e^- (+/0/-), is taken into account determining the charge from the trap occupation f_T and concentration N_T using the model in [14]. The same considerations apply to the calculation of $\tilde{\tau}_C/\tilde{\tau}_E$ for h^+.

III. INVESTIGATED DEVICES AND MEASUREMENT SETUP

In this study multi–fingered NMOS transistors, having L=4.8μm, W=10x4μm sizes, and 50Å oxide thickness, and integrated in a nanoscale technology have been used as reference devices for theoretical calculation and model validation. AC characteristics (conductance and capacitance) have been measured at a frequency ranging from 20kHz to 1MHz using a HP4284A LCR-meter and separating both the bulk and drain/source components to appropriately remove the parasitic components. The transistors have been subject to electrical stress by applying a constant gate voltage and keeping the other terminals grounded for 1000s. After the stress sequence, CV and GV characteristics have been measured again to monitor the effects of traps.
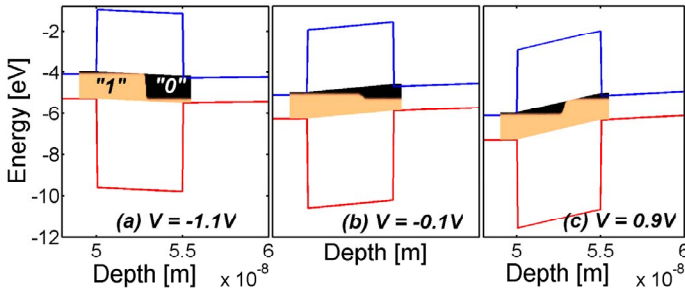

Fig. 1. Band diagrams of the simulated structure from flat-band voltage (a) to depletion (b) and inversion (c). Trap occupation f_T in the SiO$_2$ layer is also illustrated and follows the quasi-Fermi level of the gate and channel reservoirs at each equilibrium condition.

IV. CAPTURE/EMISSION FREQUENCIES AND CROSS-SECTIONS

A theoretical study of the role of the capture-emission rates dependence in energy and position has been conducted for the investigation on the underlying physical mechanisms. Figure 1 shows a scheme of the device simulated for three bias conditions and illustrating the occupation of defects in the oxide layer. For all the simulations performed in this work, it has been supposed that the traps are in equilibrium conditions with the reservoirs at the DC bias conditions. This consideration justifies the calculation of a single quasi-Fermi level for the trap distribution for both DC and AC simulations. In other words, this implies that the traps have sufficient time to reach equilibrium conditions with the gate/channel reservoirs and are able to follow the DC signal. It should be pointed out that this hypothesis is not always verified experimentally; in particular due to the wide spreading in of τ_C^{-1}/τ_E^{-1}, hysteresis phenomena can be observed (such a phenomena will be studied in a separate work)

The capture and emission frequencies calculated using Eq. 2 are shown in Figure 2 near the SiO$_2$/Si channel interface in weak
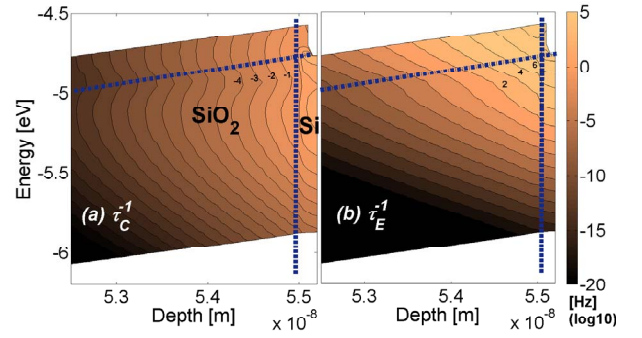

Fig. 2. Simulated capture (a) and emission (b) frequencies of electrons in weak inversion conditions (V=0.9V) as a function of the trap energy and depth in the oxide layer. A zoom of the band diagram in Figure 1 in proximity of the Si/SiO$_2$ interface is shown. Cuts in energy and depth are shown in Figure 4. The predictions of the multiphonon-assisted model show a strong decrease of capture and emission rates in oxide depth due to the reduction of wavefunction overlap and tunneling events, and energy depth due to the increase of the larger ΔE from the trap level to the energy levels in the reservoirs.
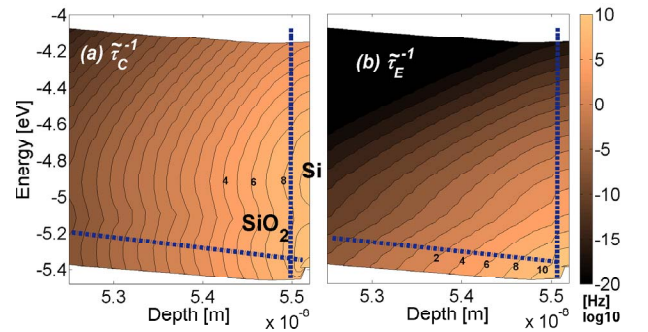

Fig. 3. Same as Figure 2 but for holes near flat band conditions (V=-0.1V).

inversion conditions. The distribution indicates the higher probability of e^- of being captured near the conduction band (in (a)) where the tunneling transition is favorable due to the overlapping of carrier and trap wavefunctions. The energy dependence is explained considering the less favorable transition of carriers when a larger amount of phonons is emitted/absorbed. The emission rates in (b) show a stronger dependence in energy given by the detailed balance of Eq. 2 as the distance with the trap energetic level to the quasi-Fermi level is exponentially reducing the emission. For the considered voltage, the oxide field remains comparable to the critical field; while moving towards strong inversion the capture frequency exponentially increase with the applied bias voltage. Similar exponential decrease in energy and position has been observed for holes capture and emission rates in Figure 3.

To further quantitatively illustrate the phenomena, the energy and depth dependencies of τ_C^{-1}/τ_E^{-1} have been plotted at the interface and at the conduction/valence band levels (Figure 4). The exponential dependence due to the wavefunction penetration in the oxide is of several orders of magnitudes stronger than in energy. It can be noticed that the point of intersection between τ_C^{-1} and τ_E^{-1} identifies the equilibrium condition of the trap with the reservoir, i.e. the calculated quasi fermi level. The e^- capture rate in weak inversion is of several orders of magnitude smaller than both the emission rate and the capture rate of holes in accumulations due to the reduced inversion charge at the considered voltage.

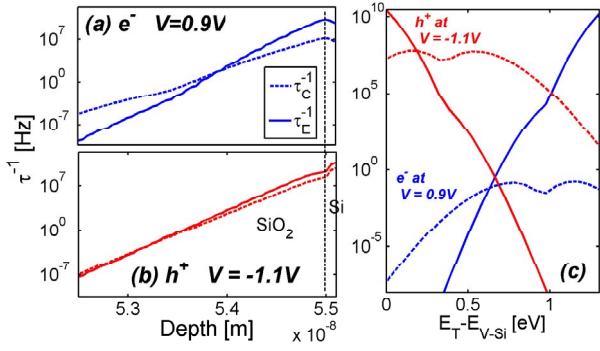The dynamics of the systems can also be described by the capture

Fig. 4. Capture and emission rates as a function of the oxide depth ((a) e^-, (b) h^+) and the trap energy (c). The capture/emission frequencies are higher near the Si/SiO$_2$ interface and in proximity of the Si valence band $E_T = E_V^{Si}$ and conduction band $E_T - E_V^{Si} = E_C^{Si} = 1.2V$. The quantities referred to h^+ are plotted for V=-0.1V while those related to e^- for weak inversion conditions at V=0.9V. The regions where the capture rate is dominating over the emission indicate the zones where the trap is occupied.

cross-section of the trap. Figure 5 shows the effective capture cross-sections simulated for different bias conditions: electrons in weak (a) and strong inversion (b), and holes in accumulation (c), flat-band (d) and depletion (e). The definition of capture cross-section [18] has been adopted: $\sigma_e = \tau_C^{-1}/(v_{th}n)$ and $\sigma_h = \tilde{\tau}_C^{-1}/(v_{th}p)$ where $v_{th} = 10^5$ m/s is the carrier saturation velocity and n and p are the mobile charge densities calculated by the Schroedinger solver. Their dependency is of considerable importance for analytical and compact models not based on physical quantum approaches.
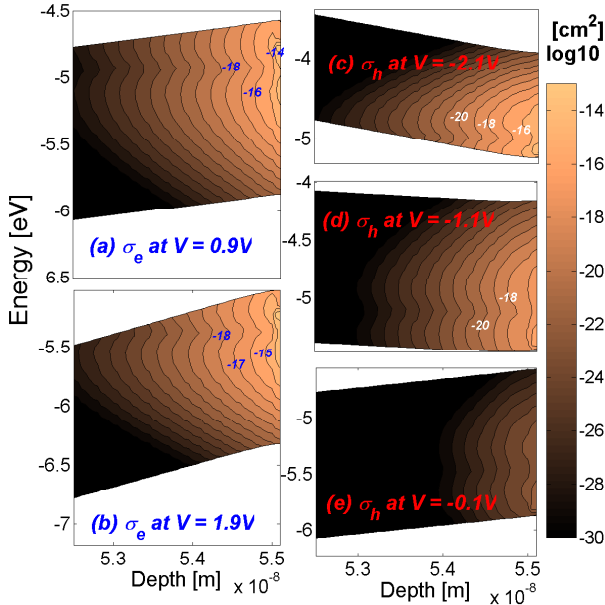

Fig. 5. Capture trap cross-sections of e^- in (a-b) and h^+ in (c-e).

V. AC ANALYSIS

The capture/emission rates of the traps have a fundamental role in the frequency dependence of both the channel capacitance C_{GC} and bulk capacitance C_{GB}. The intrinsic trap cut-off frequency τ_0^{-1}, calculated as the sum of all capture/emission frequencies [14], has been considered as the main indicator of the intrinsic trap response and its frequency dependence. Indeed, it represents the limit

in frequency at which the traps communicate with the reservoir. Its energy and position dependence has been plotted for several bias conditions in Figure 6. In other words, each iso-level in the contour plot of Figure 6 represents the limit at which traps can be characterized with a given small signal frequency. In depletion, given the large variation of capture/emission rates on several order of magnitudes, only traps near the conduction/valence bands exchange carriers and respond to the AC small signal. The accessible regions in energy and position can be easily identified in the cuts in energy and depth showed in Figure 7.
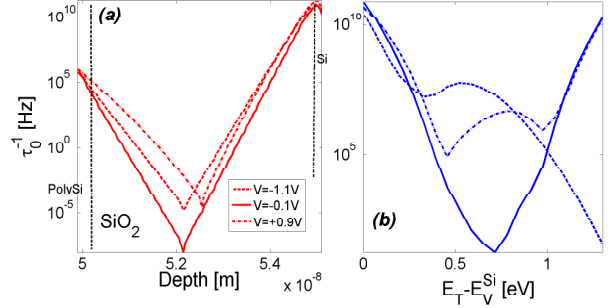

Fig. 7. Depth (a) and energy (b) dependencies of the trap response frequency τ_0^{-1}. The cuts correspond to the lines indicated in Figure 6 and are plotted for the three considered bias voltages. In (a), τ_0^{-1} is taken at the conduction band level while in (b) the results are plotted in proximity of the Si/SiO$_2$ interface. In depletion (solid line), the exponential decrease of the trap response prevents the characterization of middle-gap traps which respond with very low frequencies.
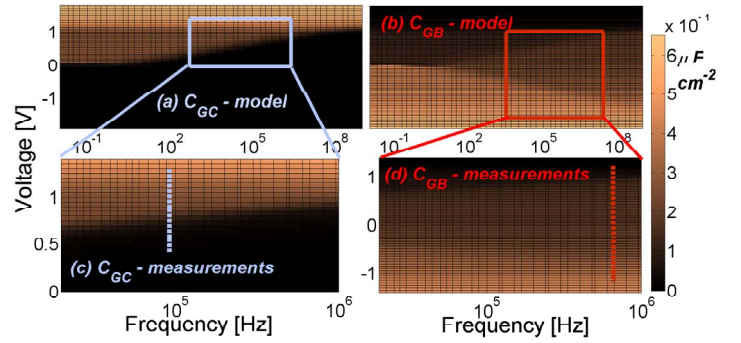

Fig. 8. Channel (a-c) and bulk (b-d) capacitances vs. DC voltage bias and small signal frequency. Model results in (a) and (b) have been plotted over a wide range of frequencies to illustrate the extreme case of trap response at very low frequencies. Both C_{GB} and C_{GC} indicate the presence of the intrinsic trap response in depletion and weak inversion and the indication of two separate bias-dependent cutting frequencies in the two regions. Simulations well reproduce measurement results over the entire frequency and bias range. The cut-off frequency on C_{GB} in weak inversion is the response of the system (bulk charges) to the trapping dynamics. A gaussian distribution of defects peaking at 2Åfrom the Si/SiO$_2$ interface and uniform in the energy bandgap from the Si conduction band to the valence band has been used to reproduce these results, in good agreement with the considerations reported in [19], [20].

Figure 8 shows the frequency and bias dependences of the measured and simulated channel capacitance C_{GB} and bulk capacitance C_{GC} characteristics on degraded devices. Several effects attributed to trapping mechanisms emerge: (1) inversion is retarded, the slope of the C_{GC} curve decreases and the threshold voltage V_{th} is subject to a shift due to negatively charged P_b centers; (2) accumulation is retarded and the curve of the C_{GB} is stretched out in the accumulation
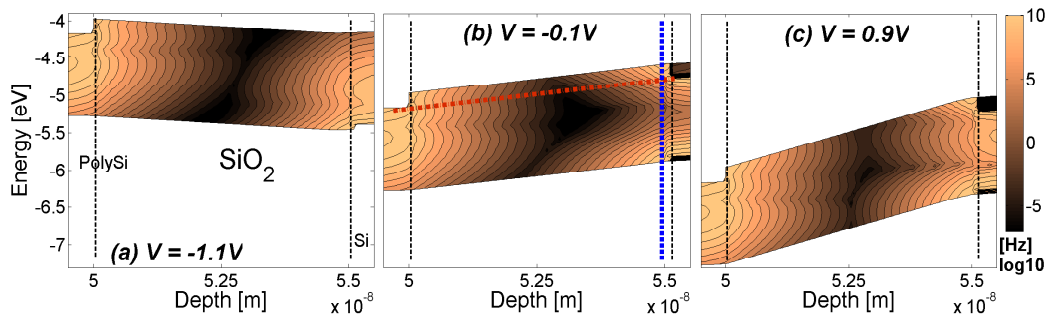
Fig. 6. Characteristic response τ_0^{-1} of the defects in the oxide layers for flat band (a), depletion (b) and weak inversion regions (c) indicating the frequency at which one trap can communicate with the gate and channel reservoir at different bias voltage. Communication is favorable in proximity of the conduction and valence bands of the Si substrate. The P_b-center model has been adopted in the entire oxide layer. However, an oxide trap model for E_γ centers has also been implemented and similar results have been obtained in terms of τ_0^{-1}. In proximity of the PolySi, traps can easily communicate with the gate reservoir, but the AC response is negligible due to their distance from the Si surface and the very low trap concentration near the PolySi/SiO$_2$ interface. Cuts in energy and depth are shown in Figure 7.

region due to positively charged P_b centers; (3) the capacitance C_{GC} presents a frequency-dependent increase in proximity of the weak/moderate inversion region; (4) the capacitance C_{GB} presents a frequency-dependent increase in depletion and near the flat band voltage V_{fb}; (5) the capacitance C_{GB} shows a frequency-dependent reduction in weak/moderate region in correspondence of the peak on C_{GC} (indeed, the substrate charge Q_B is affected by the dynamic e^- trapping during inversion). The intrinsic trap response is evidenced by the two frequency dependent peaks in depletion and weak inversion. By decreasing the frequency, one is able to scan deeper traps in energy and position following the iso-lines of τ_0^{-1} as in Figure 6. Figure 9 compares the C_{GB} and C_{GC} curves for several frequencies and evidences both the presence of the parasitic frequency-dependent peaks and the good agreement obtained with the model. The same frequency-dependent behavior can be observed on the channel conductance G_{GB} and bulk conductance G_{GC} with the presence of parasitic peaks at high frequencies representing the response of traps at the interface (Figure 10).

Fig. 10. Simulated channel (a) and bulk (b) conductances vs. DC voltage bias and small signal frequency. On $|G_{GC}|$, the peak present at high frequencies in weak inversion represents the traps AC response and is in close relation with the C_{GC} capacitance peak in weak inversion. A similar effect is present on $|G_{GB}|$ in accumulation. On the other hand, a negative peak is present in weak inversion representing the response of the electrostatics to the trapped charge response. Experimental evidence (not shown here) confirms the model results and the conductance dependencies on both bias and frequency.

multiphonon-assisted PS approach. Assessing the limitations induced by neglecting their dependence in energy and position is important for investigating the limitation of compact reliability models where an extensive use of constant cross-sections can lead to an inaccurate estimation of the trap concentration distribution. The importance of such calculation has been highlighted showing its direct application to AC analysis.
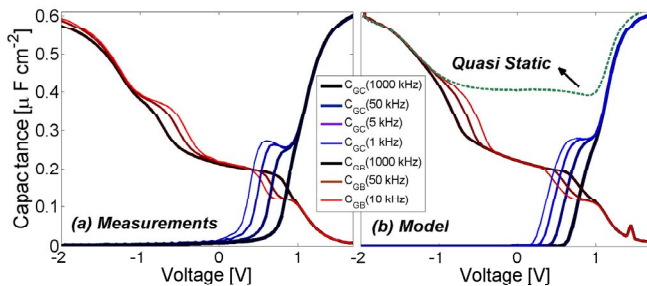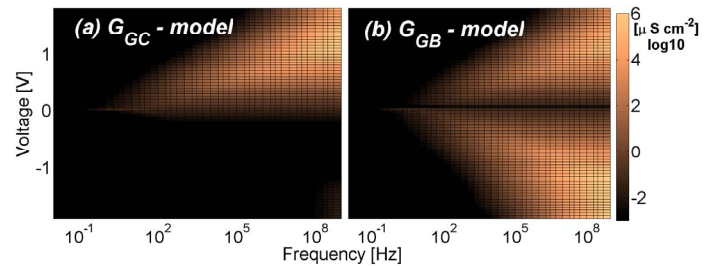

Fig. 9. Channel (in blue) and gate capacitances (in red) versus applied voltage for several small signal frequencies. The simulated results in (b) are in fairly good agreement with the measured characteristics. The cuts in frequency from Figure 8 show the parasitic capacitance due to the trap response added in the region from flat band to weak inversion. This component increases with decreasing frequency as low frequency signals are able to scan the electrical signature of traps with lower capture/emission rates. This effect is confirmed by the simulated dashed curve representing the total gate capacitance C_{GG} in the extreme case where all the traps are contributing to the AC response, and in quite good agreement with quasi-static measurements reported in [19]. The extracted total concentration of defects is $2.05 \cdot 10^{12}$cm^{-2}.

VI. CONCLUSION

A physical based determination of the interface states cross-sections for both e^- and h^+ has been performed using a

REFERENCES

[1] D. Fleetwood *et al.*, *JAP*, vol. 73, no. 10, 5058–5074, 1993.
[2] D. Ielmini *et al.*, *TED*, vol. 56, no. 9, 1943–1952, 2009.
[3] A. Palma *et al.*, *Physical Review B*, vol. 56, no. 15, 9565–9574, 1997.
[4] T. Grasser *et al.*, *Microelectronic Eng.*, vol. 86, no. 7-9, 1876–1882, 2009.
[5] D. Ielmini *et al.*, *TED*, vol. 47, no. 6, 1258–1265, 2002.
[6] K. Brower, *Physical Review B*, vol. 42, no. 6, 3444–3453, 1990.
[7] Y. Nishi, *Japanese Journal of Applied Physics*, vol. 10, 52, 1971.
[8] E. Poindexter *et al.*, *JAP*, vol. 56, no. 10, 2844–2849, 2009.
[9] E. Cartier *et al.*, *APL*, vol. 63, no. 11, 1510–1512, 2009.
[10] T. Grasser *et al.*, in *IEDM*. IEEE, 2010, 1–4.
[11] ——, *IEEE TED*, vol. 56, no. 5, 1056–1062, 2009.
[12] B. Ridley, *JP C: Solid State Physics*, vol. 13, 2015, 1980.
[13] ——. Oxford University Press, USA, 1999.
[14] D. Garetto *et al.*, in *13th International Nanotech Conference 2010*, 2010.
[15] ——, in *Proceedings of IWCE*. IEEE, 2010.
[16] V. Huard, in *IRPS*. IEEE, 2010, 33–42.
[17] T. Nguyen *et al.*, *PRL*, vol. 105, no. 22, 226404, 2010.
[18] F. Heiman *et al.*, *TED*, vol. 12, no. 4, 167–178, 1985.
[19] M. Fischetti, *JAP*, vol. 57, no. 8, 2860–2879, 1984.
[20] P. M. Lenahan *et al.*, *JAP*, vol. 55, no. 10, 3495–3499, 1984.